Paper for IESNA Annual Conference, Miami, FL, Aug. 1994, and published in J. Illum. Eng. Soc. 24(1), 106-115 (1995).

New Method for Realizing a Luminous Flux Scale using an Integrating Sphere with an External Source

Y. Ohno
Radiometric Physics Division
National Institute of Standards and Technology
A305 Metrology, Gaithersburg, MD 20899
Phone : (301) 975-2321 Fax : (301) 840-8551

Abstract

A method is proposed to realize a luminous flux scale (lumens) using an integrating sphere with a known amount of flux introduced from an external source. The integrating sphere features an opening for a detector, a test lamp in its center, a baffle between the test lamp and the detector. A second opening is used to introduce flux from an external source, and is appropriately baffled from the test lamp. Flux from the external source is introduced into the sphere through a limiting aperture of known area. The flux entering the sphere is determined from knowledge of the illuminance on the aperture plane and the area of the aperture. The total flux from the test lamp is deduced by comparison to the flux from the external source. Theoretical analysis is first made by computer simulation based on a ray tracing technique. Several integrating sphere designs are analyzed under various conditions, and based on the results of the simulation, an integrating sphere 50 cm in diameter is built to conduct experiments. The characteristics of the sphere are measured and compared with the simulation results. The total luminous flux values of several miniature lamps measured with this method are found to agree within 0.5% with measurements using goniophotometric technique. This method can be applied also to realize a total spectral radiant flux scale.

Keywords: Calibration, Computer simulation, Integrating sphere, Lumen, Luminous flux, Photometer, Photometry, Radiant flux, Ray tracing, Scale, Standards, Total Flux, Unit

---

Introduction

Total luminous flux is one of the most important measured quantities for light sources. Measurements of total luminous flux are usually performed by a substitution method using integrating spheres. The primary standards of total luminous flux are realized by using goniophotometers, usually at national laboratories. Goniophotometers, however, are often difficult to build and maintain because they require a large dark room space, a costly high-precision moving mechanism, and long hours of operation. Efforts are still continued to improve these requirements as recently reported.[1-3] Also, most goniophotometers need to rotate a lamp to be measured around one axis or more, which may cause errors for lamps which are sensitive to burning position or air drafts.[4,5] The shadow of the lamp-rotating mechanism is another problem for measuring bare lamps. There is also increasing need for spectral total radiant flux standards,[6] but the inconveniences of goniophotometers make the spectral measurements more difficult.

To alleviate such difficulties, an alternative method of realizing the total flux unit has been investigated at NIST. The method uses an integrating sphere with an opening and an external source to calibrate the total flux of a lamp inside the sphere against the known amount of flux coming into the sphere from an external source. Theoretical analysis has been made by computer simulation based on a ray tracing technique as previously reported[7].

Based on the results of the theoretical analysis, an integrating sphere of 50 cm diameter was built to verify the simulation results experimentally. The total luminous flux values measured with this method are compared with goniophotometric techniques. The approach and the results of the theoretical analysis and the experiments are discussed.

Theoretical approach

Basic design of the integrating sphere

Figure 1 shows the basic geometry of the integrating sphere designed for this purpose. The idea is to measure the total flux of a lamp inside the sphere against the known amount of the flux coming into the sphere from an external source. The input flux Φ_s (lm) is determined by using a limiting aperture at the opening of the sphere as

$$\Phi_s = E \cdot A \qquad (1)$$

where E is the average illuminance (lx) at the aperture plane, and A is the area (m^2) of the aperture. If the sphere efficiency is assumed to be spatially uniform, the total flux Φ_t of the test lamp is obtained by measuring the window illuminances for Φ_t in comparison with Φ_s.

Detector readings are compared under two conditions: when only the test lamp is turned on and when only the

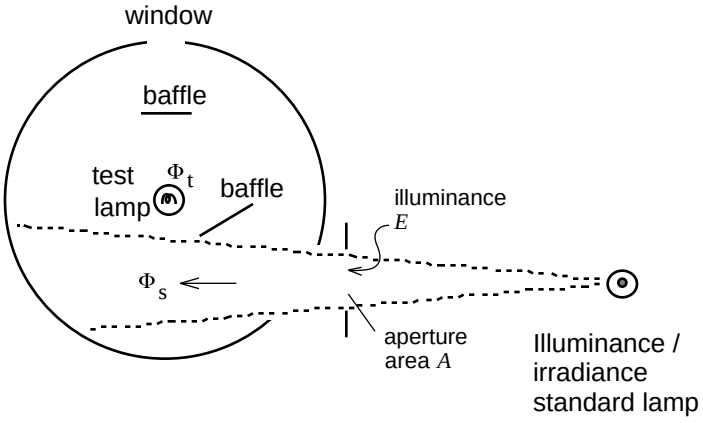

Figure 1 - Basic geometry of the integrating sphere

external standard lamp is turned on. There is no need for an auxiliary lamp to measure the self-absorption effect of the test lamp because the test lamp is kept in the sphere when measurements with the external source are made. Since the detector is exposed to most of the first reflection of the internal source, the detector should also be exposed to the first reflection of the external source to balance the sphere efficiency in both conditions. Therefore, there is no need for another baffle between the observation window and the part of sphere wall which is directly illuminated by the external source.

A possible systematic error expected in this method is the spatial non-uniformity of the sphere response caused by the two baffles and an opening. A computer simulation program has been developed to analyze this error, and to find the best geometry of the sphere design for this purpose.

Computer simulation model

The simulation program has been developed based on a ray-tracing technique and is written in FORTRAN language. **Figure 2** shows the parameters used in the simulation model. Various designs of an integrating sphere can be modeled by changing the values of these parameters. A common integrating sphere with one baffle (Ulbricht type sphere) can also be modeled by choosing R_2=R_0=0. The sphere wall is divided into 1,296 sections by θ and ϕ angles (5° x 10° step). The program calculates the illuminance and luminance to and from each section of the sphere wall and each baffle surface, so that the effect of the baffles can be accurately simulated. The interreflections are repeated until the reflected flux is almost completely absorbed, typically ~100 times for 95% wall reflectance. The program assumes Lambertian surfaces for the sphere wall and baffles. The internal source is assumed to be a point source, but simple luminous intensity distributions can be created in the program. The initial (direct) illuminance distributions on the wall are assigned so that the total flux of the test lamp and the total flux of the incoming flux are exactly the same. The window illuminances for the internal source and for the

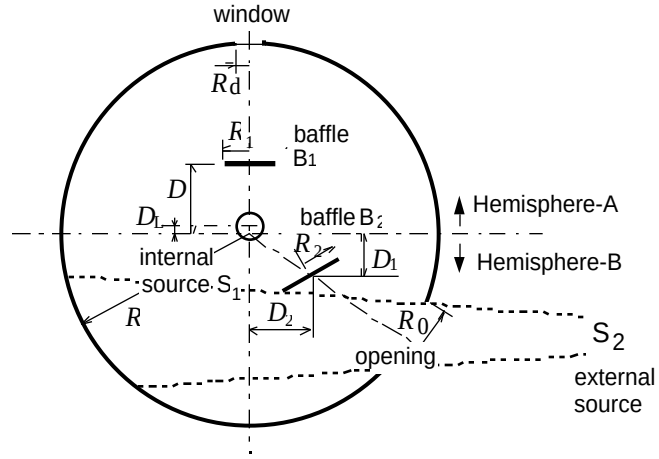

(a) Dimensional parameters

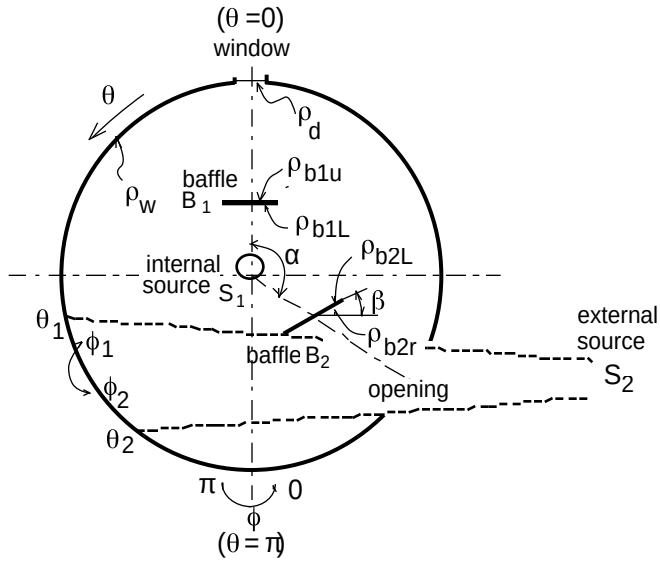

(b) Other parameters

Figure 2 - Parameters for the simulation model

external source are compared to evaluate the accuracy of this method. The details of the theory and algorithm of this simulation were previously reported [7].

Results of the simulation

Simulations are first made with an integrating sphere with various arrangements of an opening, baffles and an internal source. The simulation results are evaluated for the equivalence of the window illuminances for the internal and the external source. Of the various arrangements, the design shown in **Figure 1** shows the best equivalence.

Then, simulations are made with different values of parameters in this design to determine the optimum condition. The dimensional parameters are chosen for a practical integrating sphere to calibrate miniature lamps.

Figure 3 shows the window illuminance E_{w1} for the internal source and E_{w2} for the external source, as a function of the angle ß of baffle B_2, for varied value of reflectance ρ (0.90, 0.95 and 0.98) of the sphere wall and baffle surfaces. Both E_{w1} and E_{w2} values are normalized by the value of E_{w2} at ß = 20° for each reflectance. In this graph, E_{w1} and E_{w2} become equivalent at ß = ~70° for any reflectance value. It also shows that the difference of E_{w1} and E_{w2} is reduced significantly with higher reflectance (0.98%). It is speculated that the curve for the internal source is prominent because the luminance on the left (upper) side of baffle B_2 is

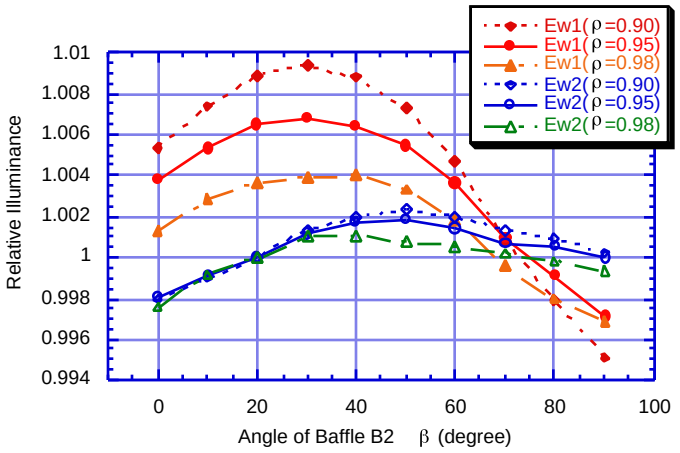

Figure 3 - Window illuminance by the internal source (E_{w1}), and by the external source (E_{w2}) for varied reflectance ρ on the sphere wall and baffle surfaces, as a function of the angle ß of baffle B_2. All the values are normalized by the value of E_{w2} at β=20° for each reflectance. Parameters: R=0.254, R_d=0.02, R_o=0.06, α=130°, R_1=0.02, D=0.09, D_L=0, R_2=0.045, D_1=0.059, D_2=0.07, θ_1=110°, θ_2=150°.

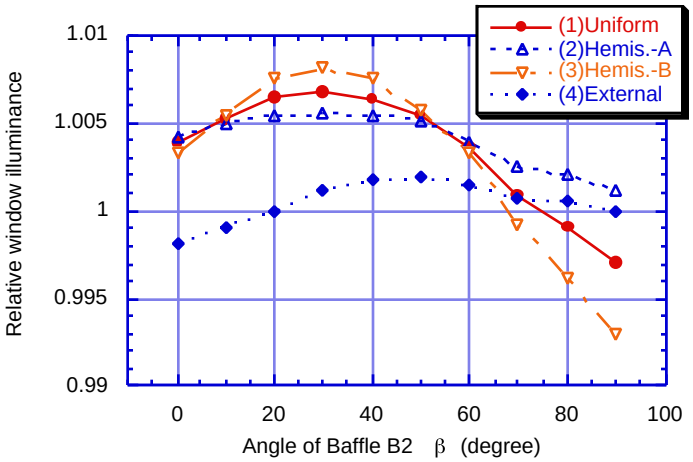

Figure 4 – Window illuminance curves with different intensity distributions of the internal source at ρ=0.95. All the values are normalized by the value of (4)External at β=20°. The sphere parameters are the same as in Fig. 3.

higher than the sphere wall. The fall-off of the window illuminance curves for larger values of ß is caused also by the change of screening effect of baffle B_2 between the window and the opening.

The errors associated with the intensity distributions of the internal source are evaluated by simulation using 1) uniform intensity for all angles, 2) uniform intensity only on hemisphere-A (See **Figure 2**a), 3) uniform intensity only on hemisphere-B, and 4) the external source. The results are shown in **Figure 4**. The parameters are the same as in **Figure 3** with ρ=0.95. All the values are normalized by the value for the external source with ß = 20°. This result shows that the errors caused by different intensity distributions of the internal source are not serious near the equivalence point (ß = ~70°).

Another simulation is made using a sphere of the same size with a smaller size opening (9 cm in diameter). Baffle B_2 is also smaller (70% in area) and its location is farther (1.44 times) from the lamp. **Figure 5** shows the results for this condition with ρ=0.95. Simulation with ρ=0.98 shows similar results. The parameter values are given in the figure caption. The results indicate that the sphere efficiency is much less sensitive to the angle β, and the calibration error (difference between E_{w1} and E_{w2}) under this condition is less than 0.1 % regardless of ß. This means that if baffle B_2 is smaller and farther from the lamp than the condition shown in **Figure 5**, the position and the angle of baffle B_2 will no longer be critical.

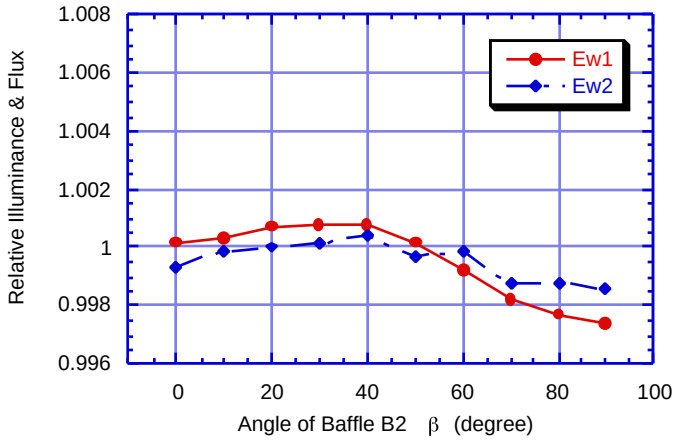

Figure 5 – Window illuminance with the small opening and small baffle B_2. All the values are normalized by the value of E_{w2} at β=20°. Parameters: R_0=0.045, R_2=0.038, D_1=0.084, D_2=0.10, θ_1=115°,θ_2=145°, ρ=0.95 Other parameters are the same as in Fig. 3.

Additional simulations are made with variations of other parameters. A simulation with a different diameter of baffle B_1 shows that the E_{w1} vs. β curve shifts down by ~0.3%, relative to the E_{w2} vs. β curve, at R_1=3 cm compared with R_1=2 cm. A simulation with varied location of baffle B_1 shows that the difference between E_{w1} and E_{w2} is almost constant in the 8 cm≤ D ≤ 16 cm range although both curves fall off significantly as distance D increases.

Experimental verification

Construction of an integrating sphere system

The theoretical analysis indicates that the sphere design described above, with parameters chosen appropriately, would have sufficient accuracy in the total flux measurement of lamps in

comparison with the flux from the external source. To verify the results of the simulation, an integrating sphere of the same design as reported in the previous section has been built to conduct experiments.

Figure 6 shows the construction of the experimental set-up. The integrating sphere has a 50 cm (20 inches) diameter, coated with barium sulfate paint of ~98% reflectance in the visible region. Two sets of Baffle B_1 (4 cm and 6 cm in diameter) and Baffle B_2 (9 cm and 7.5 cm in diameter) are made for variation of conditions. Each baffle can be placed at two different locations. Baffle B_2 is attached to a rod with a knob with an angle dial outside the sphere so that the baffle can be turned, and the angle β can be adjusted precisely. Baffle B_2 can be placed at the two locations used in the conditions of **Figure 3** and **Figure 5**. The diameter of the opening is

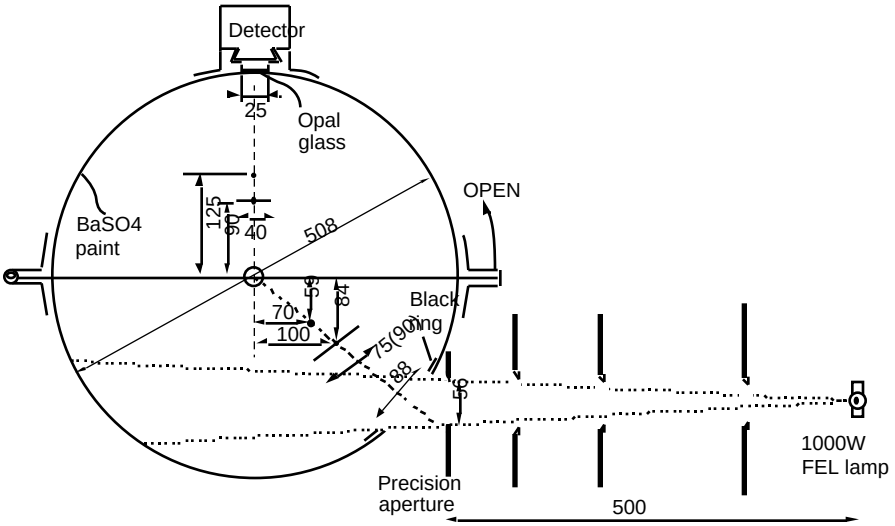

(a) Top view

Unit: mm

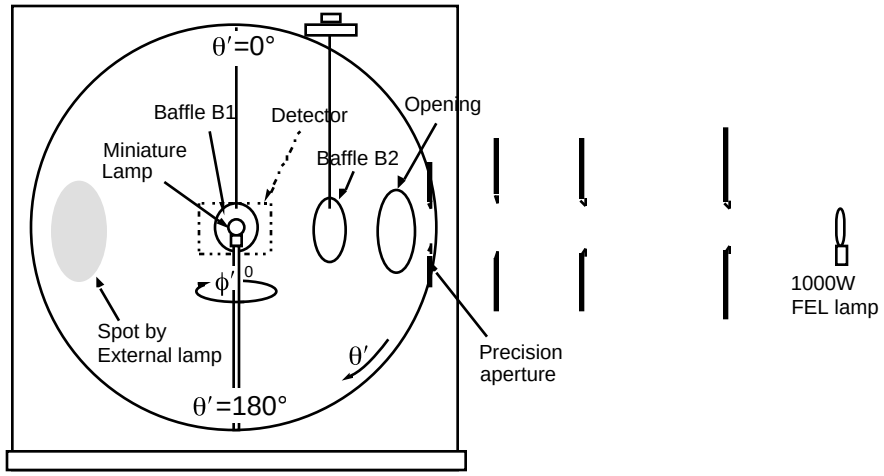

(b) Side view

Figure 6- Construction of the experimental set-up

8.8 cm (size for the condition in **Figure 5**), but when the condition of **Figure 3** (with the large opening) is tested, a flat circular ring made of black velvet, with outside diameter of 12.7 cm, is placed around the opening to mimic the larger opening. In front of the opening, outside the sphere, a limiting aperture of 5.6 cm in diameter is placed. The external source, a 1000 W quartz halogen lamp, is placed 50 cm from the aperture. To minimize stray light, screens are placed between the lamp and the aperture. The entire path from the lamp to the sphere opening is covered with black velvet cloth.

A transmitting diffuser made of ground opal glass is placed at the window of the integrating sphere. Behind the diffuser, a detector is placed which consists of a silicon photodiode and a V(λ) filter made of several layers of glass filters. The detector is contained in a temperature-controlled housing and kept at ~30° C.

Characterization of components and the system

The relative spectral responsivity of the detector has been measured in the 350 - 1100 nm region. The result in the visible region is shown in **Figure 7** (solid curve). The responsivity in the infrared region is found to be negligible. The linearity of the detector response has been measured in the 10^{-5} to 10^{-8} A range using a beam conjoiner system and found to be linear within ±0.1% in that range. The angular responsivity of the detector combined with the diffuser has also been measured. The deviation from the cosine function is less than ±1% in the 0° to 50° range of incidence angle, ~-4% at 70°, and ~-11% at 80°.

The spectral throughput of the integrating sphere with the large opening and with the small opening has been measured using lasers (Ar, Kr, tunable-dye). The laser beam is introduced into the sphere through the opening. A beam splitter and a monitor detector are used to correct for the drift of the beam power. A silicon detector with no filter is used to measure the beam power and the irradiance from the detector window with the opal diffuser. The ratio of the two readings at each wavelength gives the relative spectral throughput of the sphere. The laser power is adjusted so that the detector worked in its linearity range. **Figure 8** shows the plots of data measured at laser wavelengths. The data are interpolated in the 407 to 676 nm region, and extrapolated outside that range in the visible region, using third order polynomials obtained form the neighboring four data points. The

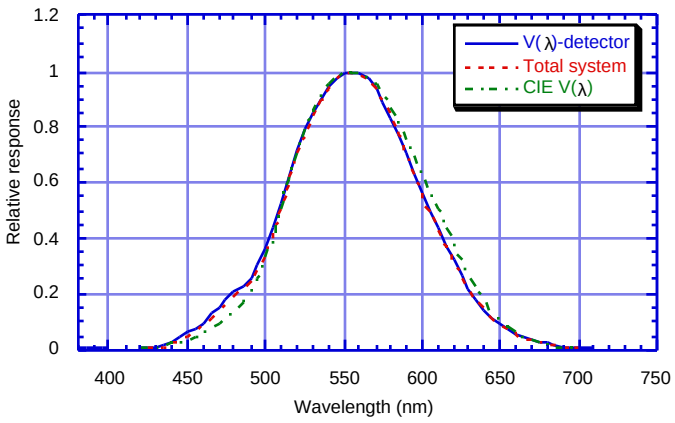

Figure 7 - Relative spectral responsivity of the detector and the integrating sphere system (the sphere, the diffuser and the V(λ)-detector).

data of the spectral reflectance of the sphere coating and the spectral transmittance of the diffuser, measured separately over the entire visible region, show a smooth curve which indicates that the extrapolation would not cause a significant error. The relative spectral responsivity of the overall integrating sphere system is calculated from the spectral responsivity of the V(λ) detector and the relative spectral throughput of the integrating sphere (with the diffuser). The obtained curve is shown in **Figure 7** (dashed curve).

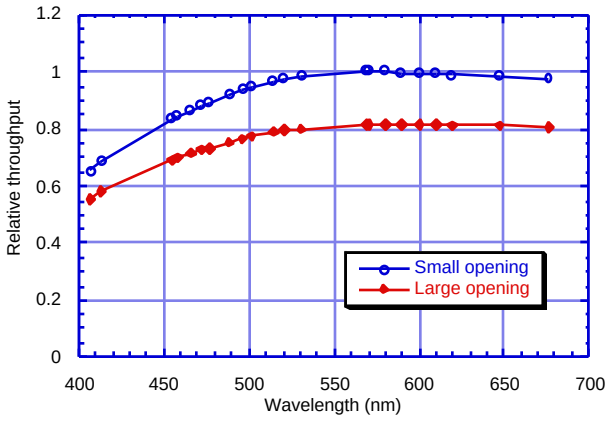

Figure 8 - Relative spectral throughput of the integrating sphere with the diffuser.

The external source is an outside-frosted 1000 W quartz halogen lamp with bi-post base, operated with base-down position. The spectral irradiance of the lamp is calibrated with the NIST spectroradiometric calibration facility[8] at a distance of 50 cm. The color temperature of the lamp is 3093 K. The orientation of the lamp is aligned using a jig (a mirror mounted on a bi-post base) and a laser. The distance from the lamp (the reference surface of the jig) to the aperture surface is measured using a length gauge. Since the solid angle subtended by the limiting aperture is not negligible, the relative luminous intensity distribution is measured over a ±3° x ±3° region in 0.5° steps. Then the relative illuminance distribution at 137 points on the aperture plane is calculated from the luminous intensity distribution, cosine factor, and distance to the lamp. The average illuminance over the aperture area is obtained from the spectral irradiance on the center of the aperture and the relative illuminance distribution data. The ratio k_a of the average illuminance to the center illuminance is 0.9975. The area of the aperture is measured at the Precision Engineering Division of NIST with an uncertainty of ±0.03% (2σ).

For the internal source to be measured, four vacuum clear-bulb miniature lamps (6V/0.2A) are used. This type of lamp is selected for its stability, its insensitivity to the burning position, and its flux level (~6 lm) which is comparable to the incoming flux from the external source (~20 lm). The relative spectral power distributions of these lamps (in one direction) are measured. The color temperature of the lamps is typically 2370 K. To correct for the error due to the mismatch of the spectral responsivity $R_{SYS}(\lambda)$ of the integrating sphere system (**Figure 7**), a color correction factor ccf_1 is calculated by,

$$ccf_1 = \frac{\int_\lambda P_2(\lambda)\, R_{SYS}(\lambda)\, d\lambda \int_\lambda P_1(\lambda)\, V(\lambda)\, d\lambda}{\int_\lambda P_2(\lambda)\, V(\lambda)\, d\lambda \int_\lambda P_1(\lambda)\, R_{SYS}(\lambda)\, d\lambda} \qquad (2)$$

where $P_1(\lambda)$ is the spectral power distribution of the internal source, $P_2(\lambda)$ is that for the external

source, and $V(\lambda)$ is the spectral luminous efficiency function. The value of ccf_1 is calculated to be 1.0173 for the large opening, 1.0177 for the small opening.

The lamps are operated using a constant current power supply. The current is controlled in the ±0.01% range (~0.08% stability in lumen output) during measurements. The lamp current is measured from a voltage across a current shunt. The detector output signal is fed to a current-to-voltage converter with a fixed gain setting.

Measurements on the effect of baffles

The simulation results indicated that the angle β of baffle B_2 has a significant effect on the sphere efficiency as shown in **Figure 3** - **Figure 5**. A series of measurements have been made to verify these results. Using the integrating sphere described above, the internal source and the external source are alternately turned on and the detector signal at each angle of baffle B_2 is measured at varied conditions.

Figure 9 shows the results of the measurements in comparison with the simulation results. It shows the plots of the window illuminance vs. angle β for the internal source and external source, with the large opening and small opening. The solid curves show the measurement and the dashed curves show the simulation results. Each curve is normalized at its peak, therefore only the shape of the curves should be compared. The experimental data at 0° with the large opening is omitted because part of the direct light from the internal source leaked from the opening. In **Figure 9**, the simulation curves agree with the experimental curves within ±0.001 which is considered to be a random error of the simulation. This result indicates that the simulation algorithm and programming is appropriate.

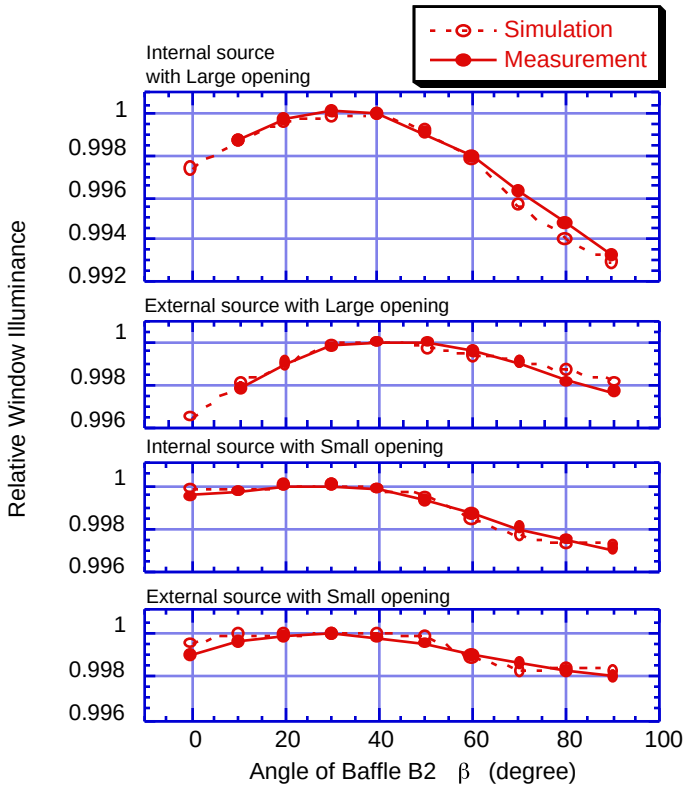

Figure 9 —— Comparison of the simulation and the measurements in the effect of the baffle B_2.

Additional measurements and simulations have been made with other conditions such as no opening for the internal source and smaller baffle B_2 with its location closer to the lamp. These additional measurements show similar agreement between the experiment and the simulation.

Comparison with goniophotometry

(a) Construction of a goniophotometer

To evaluate overall accuracy of the total luminous flux measurement using this integrating sphere system, a simple, small-size goniophotometer has been built. The total luminous flux measured with the integrating sphere system is compared with measurements by the goniophotometer.

The construction of the goniophotometer is shown in **Figure 10**. The test lamp is mounted on a horizontal pipe which is turned vertically by a stepping-motor rotation stage (scanning ϕ angle). Since the lamp is rotated, the test lamps must be burning-position insensitive. The miniature lamps used in this work are all tested in a movable light tight box with a detector and found to be ineffected by their burning position. The detector is mounted on an arm which is turned horizontally by another rotation stage. The detector scans the θ angle from -170° to +170° at each ϕ angle in the 0° to 180° range to minimize movement of the test lamp. The goniophotometer is placed in a light tight box, the inner surface of which is covered with black velvet.

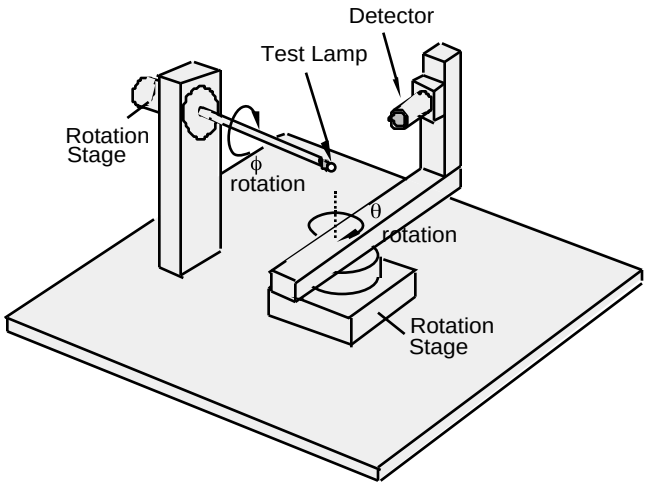

Figure 10 — Construction of the goniophotometer

The detector consists of a silicon photodiode, a V(λ) filter, a diffuser, and an aperture of 1 cm diameter. The distance from the aperture to the center of test lamp is ~20 cm. The acceptance angle of the detector is therefore 2.8°. The position of the detector was measured using a length gauge and a jig that gave the center of the rotation. A hood is attached to the detector which limited the field of view of the detector to be ~10° to minimize error by stray light. The amount of stray light is measured at several different angles by baffling the lamp by a small piece of black paper, and is found to be less than 0.2%. The detector responsivity (A/lx) is calibrated using the same quartz halogen lamp used as the external source for the integrating sphere at the same distance, 50 cm. The relative spectral responsivity of the detector is measured, and the color correction factor ccf_2 of the detector to the miniature lamps is calculated to be 0.9894 by Eq.(2) where $R_{SYS}(\lambda)$ is replaced by the spectral responsivity of the detector of this goniophotometer.

Data are sampled at 5° steps for θ and ϕ angles. The detector stops and waits 1 second before each sampling, which is long enough for the time constant of the amplifier. Measurement of one lamp takes about one hour. The signal at (θ, ϕ)=(0, 0) is taken before and after the measurement to check the stability of the test lamps during measurement. The change is less than 0.2% for all the lamps.

The detector can scan the θ angle in the range 0° to 170°, with 10° dead angle near the support pipe. The miniature lamps used in this work are of clear-bulb type and there is a shadow of the base in the θ area of ~150° to 180°. The luminous intensity of the miniature lamps falls off

at θ=170° to less than 0.13% of the average value (lumen/4π). Also, considering the solid angle of the dead angle region, which is only 0.76% of 4π, the error due to the dead angle in this case is negligible.

(b) Analysis on the spatial non-uniformity of the integrating sphere

Although the simulation predicts the effects of baffle B_2 and the opening accurately, the simulation is still dealing with an ideal sphere with Lambertian surface and no contamination on the bottom part of the sphere. Another difference to be noted is that the experimental sphere used in this work has a gap of ~1 mm width between the two hemispheres when the sphere is closed. The dimensional parameters of the sphere may also be slightly different due to the fabrication accuracy. Since the external source irradiates the area of the sphere wall with no gap and less contamination, the sphere efficiency for the internal source is considered to be slightly lower than what is predicted by the simulation.

To clarify this point, the spatial non-uniformity of the sphere response has been measured by rotating a miniature lamp of the same type, on which a hood is attached to produce a uniform irradiation only within ~45° beam angle (a circular spot of ~20 cm in diameter on the sphere wall). **Figure 11** shows the plots of relative detector signals for the beam spot turned from $\phi'=0$ to 360° at 45° intervals, at each θ' angle from 0° to 180° at 45° intervals, a total of 26 points. The (θ',ϕ') coordinate is shown in **Figure 6** (b), which is different from the (θ, ϕ) coordinate in **Figure 2**. The measurement interval is fairly large due to the limited instrumentation, but it is matched to the beam angle of the source to minimize errors. **Figure 11** clearly shows the effect of the gap and slight contamination on the lower part of the sphere wall. Let $K(\theta',\phi')$ be the relative detector signal, the sphere efficiency k_1 for the internal source (assumed as a point source), relative to $K(0,0)$, is expressed by

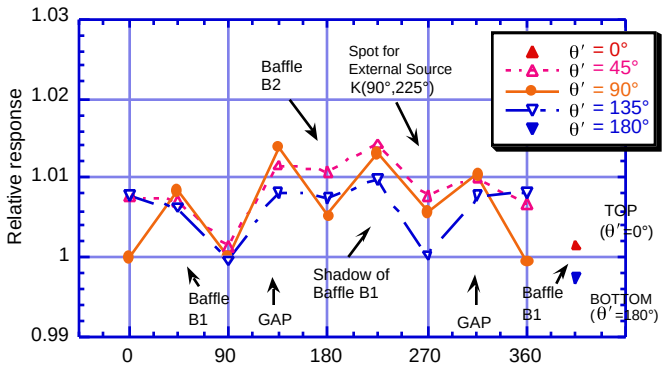

Figure 11 — Spatial non-uniformity of the sphere efficiency. (θ', ϕ') coordinate is shown in Fig. 6 (b). $\phi'=0$ is the direction to the detector. The values are normalized at (90°, 0°).

$$k_1 = \sum_{\theta=0°}^{180°} \bar{k}(\theta)\,\Omega(\theta)\,\Delta\theta \;/\; \sum_{\theta=0°}^{180°} \Omega(\theta)\,\Delta\theta \qquad (3)$$

where

$$\bar{k}(\theta) = \sum_{\phi=0}^{360°} K(\theta,\phi)\,\Delta\phi \;/\, 360°$$

$$\Omega(\theta) = 2\pi\{\cos(\theta-\Delta\theta/2) - \cos(\theta+\Delta\theta/2)\} \quad \text{for} \quad (\theta\neq 0,\ 180°)$$

$$\Omega(\theta) = 2\pi\{1-\cos(\Delta\theta/2)\} \quad \text{for} \quad (\theta=0,\ 180°)$$

$$\Delta\theta = \Delta\phi = 45°$$

The relative sphere efficiency k_2 for the external source is given as $k_2 = K(90°, 225°)$. The ratio k_1/k_2 is calculated to be 0.994. Therefore, a spatial non-uniformity correction factor k^* ($=k_2/k_1$) is applied to the results of the miniature lamps measured with the integrating sphere.

(c) Comparison of the total luminous flux measurements

The total luminous flux of four miniature lamps has been measured three times using the integrating sphere system mentioned above. The total luminous flux Φ_t of a miniature lamp is obtained by,

$$\Phi_t = y_1 \cdot ccf_1 \cdot k^* \cdot E \cdot k_a \cdot A / y_2 \qquad (4)$$

where y_1 is the detector signal for the internal source, ccf_1 is the color correction factor, k^* is the sphere efficiency nonuniformity correction factor, E is the illuminance by the external source on the center of the aperture plane, k_a is the illuminance nonuniformity correction factor, A is the area of the aperture, and y_2 is the detector signal for the external source.

The total luminous flux of each lamp was also measured three times by the goniophotometer mentioned above. The total luminous flux is obtained from the measured average luminous intensity at each polar angle and the zonal constants, with color correction factor ccf_2 applied. **Figure 12** shows the plots of the sphere measurements (with the small opening condition, β=70°) and the goniophotometer measurements. The sphere measurements were also made with the large opening condition (β=70°), and very similar results were obtained. The total flux values of the miniature lamps measured with the two methods agreed within 0.45 %, the average difference being 0.26 %.

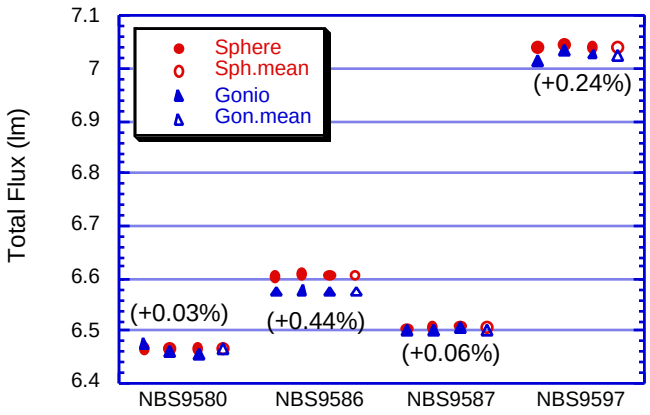

Figure 12 — Results of the comparison of the total luminous flux measurements by the sphere method (with the small opening, β =70°) and by the goniophotometry . The numbers in parenthesis show the difference of the mean values of the two methods.

Uncertainty analysis

The uncertainty factors of the integrating sphere method include the reproducibility of measurements for the external lamp (0.1 %), the uncertainty of the distance setting (0.2 mm, 0.08 % in photometric uncertainty), the uncertainty of the aperture area (0.05 %), color correction uncertainty (0.1 %), the reproducibility of internal lamps (0.2 %), and the uncertainty of the correction factor k^*(0.3 %) - all are 2σ uncertainties. The diffraction loss at the aperture is calculated to be negligible. The overall uncertainty (expanded uncertainty, k=2) relative to the spectral irradiance lamp is estimated to be 0.4 %.

The uncertainty factors of the goniophotometer include the uncertainty of the detector

responsivity calibration relative to the spectral irradiance lamp (0.1 %), uncertainty of distance setting from the detector to the center of rotation (0.2 mm, 0.2 % in photometric uncertainty), stray light (0.2 %), color correction uncertainty (0.1 %) and reproducibility of results (0.3 %) - all are 2σ uncertainties. The reproducibility of results is based on the maximum standard deviation when the goniophotometer measured the same lamp repeatedly with remounting the lamp with different orientations of the filament. The deviations are due to the reproducibility of both the goniophotometer and the lamp. The overall uncertainty (expanded uncertainty, k=2) of the goniophotometer relative to the spectral irradiance lamp is estimated to be 0.5 %. The disagreement of total flux values between the two methods reported above is within the uncertainty range of this comparison measurement.

The uncertainty of the spectral irradiance lamp is not discussed here because both the integrating sphere and the goniophotometer are calibrated against this lamp. The error in the calibration of this lamp should be canceled out in the comparison results reported above.

Conclusion

The experimental results on the effect of baffle B_2 agree with the simulation results, which indicates that the simulation program has sufficient accuracy in predicting the effects of the baffles. The comparison of absolute measurements of total luminous flux also shows acceptable results, which proves that this simulation technique is useful for the design of integrating spheres.

The simulation program of the current version, however, does not consider non-uniformity of reflectance on the sphere wall, non-Lambertian characteristics of the sphere coating, gaps between hemispheres, etc., which exist more or less in any actual integrating spheres. It would be necessary to incorporate calculations for these factors to further improve the accuracy of the simulation.

The total luminous flux measured with the integrating sphere method agrees with the goniophotometric technique within 0.5%, which verifies that the integrating sphere method has sufficient accuracy with all the corrections adequately applied. The uncertainty of the measurement can be improved by using an integrating sphere of larger size, with smaller opening and smaller baffles relative to the size of the sphere. The spatial nonuniformity correction factor k^* can also be measured more precisely with a larger sphere at smaller intervals. The overall uncertainty can also be reduced by using standard photometers to determine the average illuminance on the aperture plane directly.

This method will be applied using a 2 m integrating sphere to realize a luminous flux scale based on the detector-based candela scale[9] at NIST. We also plan to investigate the application of this method to the total spectral radiant flux measurements.

The author would like to express his thanks to K. D. Mielenz and D. A. McSparron for their guidance in this research. Thanks are also due to R. D. Saunders who offered support in the spectral throughput measurements, and to C. McCarter at Hoffman Engineering who provided an integrating sphere for this work.

Reference

1. Bastie, J.; Andasse, B.; Foucart, R. 1991. Luminous flux measurements with a goniophotometer; study of time effects on data collection. *CIE Proceedings 22nd Session*, 1-1, Division 2 :45-47
2. Hu, R.S. 1991. Importance of axis alignment in goniophotometry. *CIE Proceedings 22nd Session*, 1-1, Division 2: 21-22
3. Lewin, I.; Laird, R., Carruthers, B. 1990. Development of new photometer concepts for quality control applications. *J.IES*, 19-2 : 90-97
4. Levin, R.E. 1982. Photometric connection, *LD&A*, 12-9 :28-35
5. Otsuka, T.; Hatanaka, H.; Sakaguchi, T.; Fukuhara, M., and Noguchi, T. 1991. A study on the photometric measurement of floodlights. *CIE Proceedings 22nd Session*, 1-1, Division 2 : 3-4
6. Goodman, T.M.; Moore, J.R.; Pearce, N.C.; Murray, D.K. 1991. The establishment of a new national scale of spectral total flux. *CIE Proceedings 22nd Session*, 1-1, Division 2 : 50-53
7. Ohno, Y. 1994. Integrating sphere simulation: Application to total flux scale realization. *Applied Optics* 33-13: 2637-2647. (to be published)
8. Walker, J.H.; Saunders, R.D.; Jackson, J.K.; and McSparron, D.A. 1987. Spectral Irradiance Calibrations. *NBS Special Publication 250-20*. National Bureau of Standards, Gaithersburg MD.
9. Ohno, Y. 1994. The detector-based candela scale and related photometric calibration procedures at NIST. *J.IES* 23-1 : 89-97.